PROBLEMS OF MECHATRONICS
ARMAMENT, AVIATION, SAFETY ENGINEERING

ISSN 2081-5891 **2 (4), 2011, 7-28**

Specific Design Features of Solid Propellant Rocket Motors for Shoulder-Launched Weapon Systems*

Berko ZECEVIC, Jasmin TERZIC, Mario BASKARAD,
Alan CATOVIC, Sabina SERDAREVIC-KADIC and Zijo PEKIC

University of Sarajevo, Mechanical Engineering Faculty,
Defence Technologies Department
Vilsonovo setaliste 9, 71000 Sarajevo, Bosnia and Herzegovina

Abstract. Solid propellant rocket motors for Shoulder Launched Infantry Weapon Systems (SLWS) are characterized with a very short burning time, high-pressure combustion and a wide spectrum of design solutions for rocket motor structure. Interior ballistic behaviour of such rocket motors depends on many factors such as design structure, propellant grain shape, propellant grain joint to the rocket motor case, type and location of the igniter, spinning mode and nozzle design. Erosive burning also plays important role due to high combustion gases mass flow rate. Numerical simulation of the igniter combustion gases flow through the hollow of the propellant grain tubes with gas temperature distribution was carried out in this paper. Results confirmed assumptions that igniter interior gas flow affected duration of the pressure rise. A mathematical model approach for prediction of the curve p = f(t) which was included in a model of the corrected propellant grain burning surface for two types of short-time rocket motors has been presented. A good agreement with measured curves was achieved.
Keywords: short-action solid rocket motor, burning rate, ignition time, derivative *dp/dt*, regression model

* Presented at 8th International Armament Conference on „Scientific Aspects of Armament and Safety Technology", Pułtusk, Poland, 6-8 October, 2010.

1. INTRODUCTION

An intensive development of shoulder-launched weapon systems (unguided and guided) with munitions propelled by solid propellant rocket motors has been taking place recently. These projectiles have a range of several hundred meters up to approximately 800 meters. Current shoulder fired missiles and rockets are designed primarily to defeat tanks and armoured vehicles, but are inadequate when fired against brick walls or fortified concrete targets.

The shoulder-fired man-portable anti-tank missile systems usually use gas generators in order to launch a rocket from a launch tube or booster rocket motors that are separated after launching. Some of them have a booster rocket motor which is integrated into the missile structure. Typical representatives of shoulder-fired man-portable anti-tank missile systems are the M47 DRAGON, ERYX, FGM-148 Javelin, Spike-SR etc.

At unguided SLWS, solid propellant grain must be burnt while a projectile is still inside the launch because of operator’s safety requirements. Typical representatives of shoulder launched infantry rocket weapons include the Apilas, the Shoulder-launched Multipurpose Assault Weapon (SMAW), the M72 LAW Light Anti-Armor Weapon, the 64 mm M80 Zolja, RPG-18, LAW 80 Light Anti-Armor Weapon, B-300, RPG-22, RPG-26, Shipon, 90 mm M79 OSA etc.

A common feature of both types of SLWS is a rocket motor with an extremely short burning time, measured in milliseconds.

Acceleration during the launch phase makes another distinction between SLWS; guided anti-tank missiles have a low acceleration when launched while unguided infantry projectiles have an acceleration of 3000-8000 g. These distinctions affect design of the entire rocket motor, especially the nozzle.

Design of solid propellant rocket motors for SLWS munitions is considerably more complex compared to most of rocket motors used for other purposes. Specific requirements for such rocket motors are as follows:

- Short burning time;
- Launch rocket motor must not be active at the launch tube muzzle;
- High pressure inside the rocket motor chamber;
- Environmental conditions during use from −40°C up to +60°C;
- Low temperature sensitivity of the solid propellant;
- Reliable ignition;
- Short ignition time;
- Short ignition rise time.

High safety requirements, because SLWS is fired from the operator’s shoulder. Rocket motors for SLWS missiles have small dimensions and weight when compared to a total weight and mechanical envelope of the missile. An envelope of the rocket motor is not dominant at missile design structure.

Fig. 1. A Soldier fires an AT-4 Weapon at a target [1]

At SLWS rocket munitions, nozzle is dominant within the envelope of the rocket motor. The following figures show characteristic mechanical envelopes of short-time combustion rocket motors, B-300 or SMAW, APILAS and ACL APX-80. It can be seen that the nozzle throat diameter is quite big, the nozzle expansion ratio is low and the rocket motor occupies a significant part within a mechanical envelope of the entire rocket projectile. Nozzle design indicates that combustion products mass flow through the nozzle is extremely high. Such flow conditions induce erosive burning of the propellant grain particularly in the start-up phase.

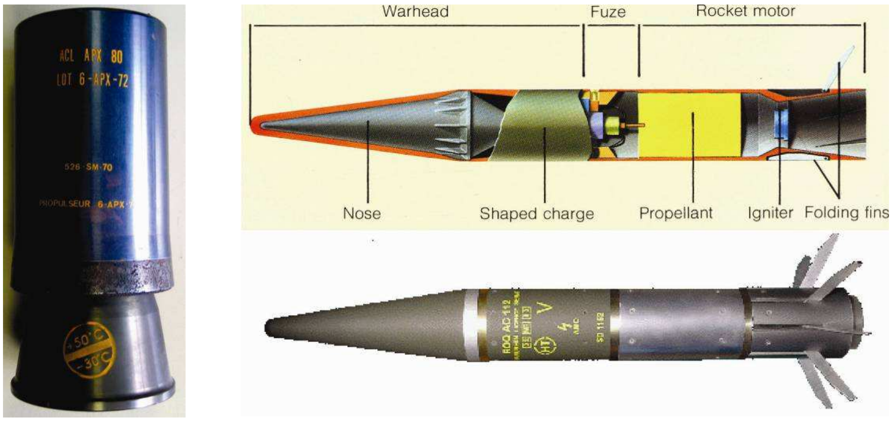

Fig. 2. The ACL APX-80 rocket motor (left) and the APILAS rocket motor [2] (right)

High exhaust mass flow generates overpressure blast behind the launcher (Figure 1) which is a specific problem when an SLWS is fired from a closed area. This is the main deficiency of most current weapons because they cannot be fired from enclosures, such as rooms or bunkers, rendering the user vulnerable to enemy fire. This problem is also important for design of short burning time rocket motors applied in SLWS.

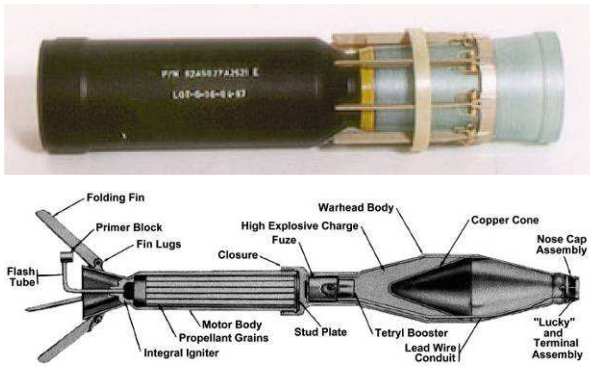

Fig. 3. The B-300 rocket motor [3] (up), the 66 mm M72 LAW rocket [17] (down)

This brief overview has described most significant influences, resulted from intended use of SLWS, on design of rocket motors.

2. PUBLISHED DATA OF SOME SHORT-ACTION SOLID PROPELLANT ROCKET MOTORS

The published papers describing available which describe a specific methodology for designing of short time rocket motors are quite rare. The Mechanical Engineering Faculty, University of Sarajevo – Defence Technology Department has carried out a comparative analysis of four short burning time rocket motors in order to explore some specific design features of rocket motors for SLWS, which would make a distinction between them and general design features of tactical solid propellant rocket motors.

Two rocket motors from the SLWS DRAGON (gas generator, Figure 5 and correction impulse rocket motors, Figure 4.), the 68 mm “Zolja” rocket motor (similar to the M72 LAW or the RPG-18) and the 90 mm “OSA” rocket motor were analysed in this paper.

The DRAGON is a SLWS which consists of a launcher, tracker and a medium-range, wire-guided antitank missile [4]. The gas generator mounted inside the rear part of the launch tube serves as a High-Low pressure propulsion system.

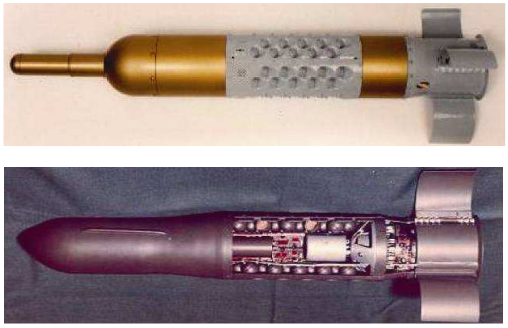

Fig. 4. Impulse control rocket motors of the DRAGON missile [18]

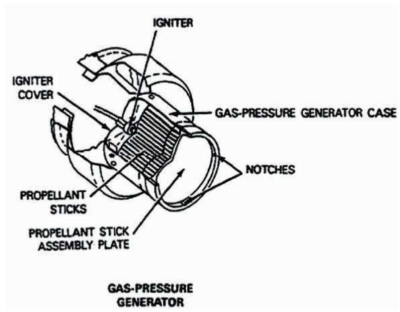

Fig. 5. Gas generator of the DRAGON missile [4]

High pressure of 17-24 MPa develops inside the gas generator structure, while low pressure of 1,7-2,1 MPa forms inside the launch tube. The gas generator enables launching of the DRAGON missile from the launch tube.

Control is performed by means of plurality of small correction impulse rocket motors mounted around the cylindrical body of the missile.

The gas generator propellant grain made of the M36 double base propellant is in the form of 190 tubular sticks, which are bonded to an aluminium propellant holder. The M-36 propellant has high burning rate, mesa burning characteristics over operating pressure range, low π_K, high specific impulse, it is smokeless and easy to manufacture.

From firing test curves $p = f(t)$ for the DRAGON's gas generator conditioned at temperatures of 233 K, 294 K and 336 K (Figure 6 and 7) following characteristics are distinct:

- Ignition delay time is quite long when compared with total action time;
- Pressure rise at start-up phase is high (dp/dt achieves 70 MPa/ms at a temperature of 336 K, and 13 MPa/ms at a temperature of 233 K);
- Ignition rise time is short (mean ignition rise time 4,398 ms for 233 K);
- Mean combustion time (action time) is between 25,43 ms (for 336 K) to 31,311 ms (for 233 K);
- Tail-off phase is significantly longer then the start-up phase.

In order to estimate specific points from pressure vs. time curve $p = f(t)$, which is used to determine ignition delay, ignition rise time, combustion time (action time) and tail-off time, a digital processing of $p = f(t)$ curves has been applied at the Defence Technology Department. Curves $p = f(t)$ were transformed into $dp/dt = f(t)$, from which all characteristic points are easier to be noted. Derived dp/dt vs. time curves clearly indicate characteristic phases of the rocket motor action and influence of conditioned temperatures on combustion chamber pressure variation particularly during transient start-up and tail-off phases.

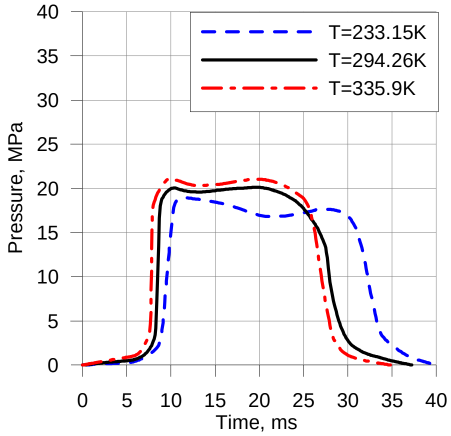

Fig. 6. DRAGON gas generator pressure vs. time [4]

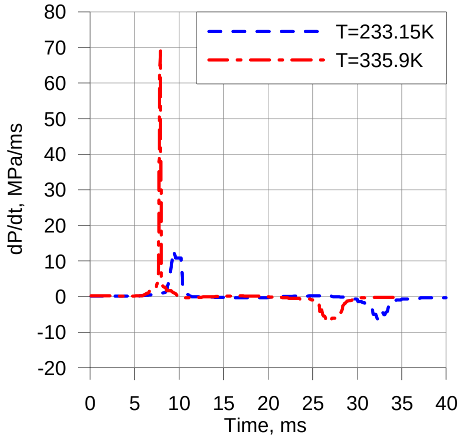

Fig. 7. DRAGON gas generator dp/dt vs. time

Impulse rocket motors of the DRAGON missile use the same M36 solid propellant (as in the gas generator) which is formed into strips and then is rolled into cylinders. Analysing published firing test curves $p = f(t)$ for conditioned temperatures of 233 K, 294 K and 336 K (Figure 8) by means of derivative $dp/dt = f(t)$ (Figure 9), following characteristics can be noticed:

- Transient processes are short when compared with total action time of the rocket motor (f. e. mean ignition delay time is 1,88 ms for 233 K);
- Pressure rise at start-up phase is also high (*dp/dt* achieves 65 MPa/ms at a temperature of 336 K, and 17 MPa/ms at a temperature of 233 K);
- Ignition rise time for all temperatures is extremely short (mean ignition rise time is 0,69 ms at 233 K);
- Mean combustion time (action time) is 24,16 ms (for 233 K) to 18,60 ms (at 336 K);
- Peak pressure of 36,21 MPa, occurred at the end of burning at a temperature of 336 K, was most likely caused by cracking of the solid propellant grain, because there were no same occurrence at other two conditioned temperatures;
- Although the propellant type is the same as in the gas generator with similar webs (1,04 mm vs. 1,17 mm), a higher sensitivity to temperature was noticed when compared with gas generator pressure-time behaviour. It means that solid propellant grain shape, rocket motor design structure and burning conditions affect the burning process;
- Derived curves *dp/dt* vs. time also indicate characteristic phases of the rocket motor action and considerable influence of conditioned temperatures on combustion chamber pressure variation particularly during transient start-up and tail-off phases.

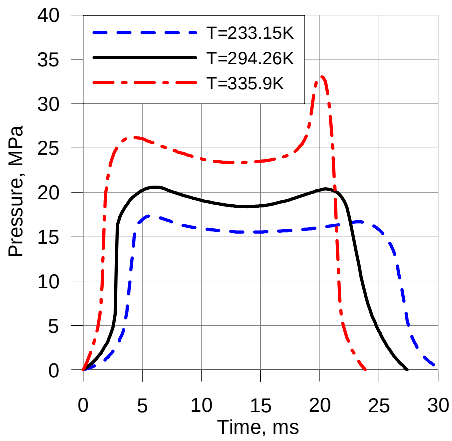

Fig. 8. DRAGON impulse control rocket motor pressure vs. time [4]

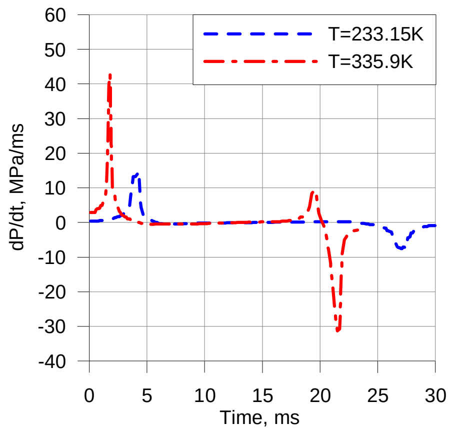

Fig. 9. DRAGON impulse control rocket motor dp/dt vs. time

Ignition delay (time when 10% of initial peak pressure is achieved) is determined by burst diaphragm design features. Greater thickness of the burst diaphragm can cause combustion oscillations, unforeseen peak pressure and even solid propellant grain to be cracked. Thinner burst diaphragm could affect harder ignition particularly at lower temperatures as 233 K, so this problem should be taken into consideration when a new rocket motor is designed.

Fig. 10. 64 mm M80 rocket motor (above [19]) and its multiple tube grain (down)

Since more detailed design data about the above described rocket motors were not available for further analysis, our efforts were focused on the SLWS rocket motors with known design features.

These are two SLWS rocket motors using double base propellants with almost the same propellant composition but with different propellant grains.

The rocket motor of the 64 mm HEAT M80 rocket (Figure 10) contains solid propellant grain made of a double base NGR-124 propellant, which is in the form of multiple-tube grain with 37 tubular sticks bonded to an aluminium propellant holder.

By analysing firing test curves $p = f(t)$ for conditioned temperatures of 243 K, 294 K and 323 K using $dp/dt = f(t)$ derivative, following characteristics can be noticed (Figure 11):

- A strong temperature sensitivity of the propellant to temperature is obvious – action time of the rocket motor is about 10 ms at a conditioned temperature of 243 K and about 5 ms at 323 K;
- Ignition rise time is quite long and it is almost as web burning time;
- Start-up pressure rise is quite unusual at a temperature of 233 K;
- During the ignition phase, maximum value of *dp/dt* at a temperature of 323 K is 38 MPa/ms, while it is only 5 MPa/ms at 223 K;
- Pressure rise at the start-up phase is pretty modest at 233 K, which means that the ignition process was not optimal for design structure of the rocket motor (burst diaphragm adhesive joint affects the ignition process at various temperatures, which is outstanding at low temperatures);
- Tail-off time is less then the start-up ignition rise time, which is unusual for rocket motors.

The burning process is affected by grain geometry and propellant type, rocket motor chamber design, ignition case, mass and type of ignition charge etc.

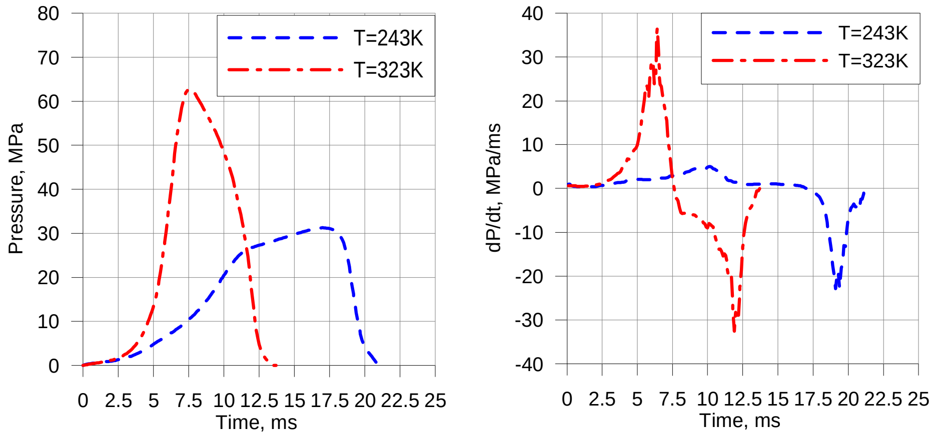

Fig. 11. Pressure vs. time curve and dp/dt vs. time for rocket motor of 64 mm HEAT M80

The rocket motor of the 90 mm HEAT M79 rocket (Figure 12) contains a solid propellant grain made of a double base NGR-114 propellant, which is in the form of multiple-tube grain with 121 tubular sticks bonded to an aluminium propellant holder.

Fig. 12. 90 mm M79 rocket motor (left) and its hollow cylindrical type propellant grain (right)

By analysing firing test curves p=f(t) for conditioned temperatures of 243 K, 294 K and 323 K using derivative $dp/dt = f(t)$ (Figure 13), the following characteristics of this rocket motor can be noticed:

- High temperature sensitivity reflecting through the rocket motor action time (about 13 ms at 243 K and about 7 ms at temperature of 313 K);
- Ignition rise time is quite long when compared with total burning time, particularly at a temperature of 313 K;
- Maximum value of *dp/dt* at temperature of 313 K at start-up phase is 33 MPa/ms, while it is 19 MPa/ms at 243 K;
- Tail-off phase time is unusually long at a temperature of 243 K, indicating that the rocket motor design was not optimised;
- Pressure rise at the start-up phase is quite slow at 243 K, which also means that ignition process was not optimal for design structure of the rocket motor;
- Tail-off phase time at temperature of 243 K is distinctly long and variation of derivative *dp/dt* behaves unexpectedly.

Solid propellant composition, shape and dimensions of the propellant grain for both rocket motors are very similar, but considerable variations in the interior ballistic processes were noticed. As already mentioned, the long start-up phase of the 64 mm „Zolja” rocket motor (at a temperature of 243 K) indicates a considerable influence of the igniter as well as entire rocket motor design on interior ballistic of short-action rocket motors. Therefore, it is important to explore an influence of erosive burning (during the start-up phase), temperature sensitivity of the propellant, ignition process and design of interior rocket motor structure on interior ballistics of these rocket motors.

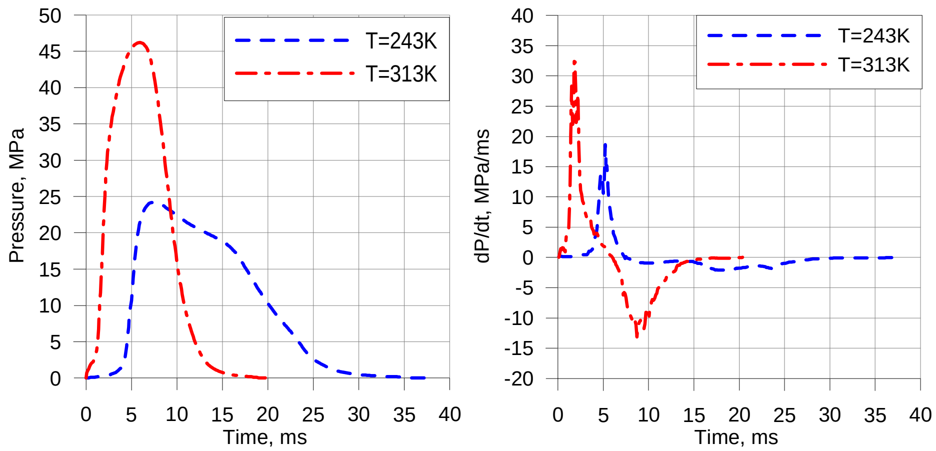

Fig. 13. Pressure vs. time and dp/dt vs. time for the rocket motor of the 90 mm HEAT M79

3. ANALYSIS OF ROCKET MOTORS 64 MM M80 AND 90 MM M 79

Short-Action solid propellant rocket motors are characterized by a short burning time, high propellant loading density and significant influence of erosive burning at the start-up phase.

In order to explore an influence of some parameters on interior ballistics of short-time rocket motors it is necessary to determine the burning rate law using ballistic evaluation motors, as well as using actual rocket motors (where erosive burning is included), including ratios $K = A_b/A_{th}$ (where A_b = burning propellant surface, A_{th} = nozzle throat area), $K_i = A_b/A_p(x)$ ($A_p(x)$ = Cross-sectional area or port area available for the downstream gas flow) and $J = A_{th}/A_p(x)$.

For rocket motors with high loading density, the total port area in the grain available for the downstream gas flow usually becomes very small, however, there is a certain limit that must be taken into account to avoid burning instabilities. This geometrical condition is most important at the beginning of the combustion process because the total port area of the grain is minimal and can be characterized by the value of $K_i = A_b/A_p(x)$. After ignition, an initial value for K_i should be limited to $J_i = K_i/K < 0{,}6$ in order to avoid burning instabilities.

For a multiple-tube grain the definition of the different values for K_i can be helpful to characterize the axial flow in the combustion chamber, the first of which is formulated with the total cross-section port area, the second with all wedge shaped cross-sections between the tubes and the third, generally the most critical one, with the port area of a single tube and the appropriate burning surfaces which generate the local downstream gas flow [5].

The basic multiple-tube grain configuration can be found and optimised by using a special Dynamit Nobel computer software which includes the grain geometry related aspects of internal ballistics and offers the user a choice of geometrical tube arrangements. Multiple-tube arrangement in combustion chambers with ring-shaped cross-section can also be handled with this software. For tubes arranged in concentric circles, the inner diameter *R* of a rocket motor case can be easily expressed as a function of the grain tube diameter *r*. Table 1 contains this relationship ($R = r \cdot x$) together with the loading factor [5].

Table 1. Multiple-Tube Grain Design Parameter

No. tubes	x	Loading factor
3	2,155	0,6462
4	2,414	0,6864
5	2,701	0,6852
6	3,000	0,6667
7	3,000	0,7778
8	3,306	0,7320
9	3,613	0,6895
10	3,924	0,6494
11	4,236	0,6130
12	4,232	0,6700
13	4,236	0,7244
15	4,552	0,7238
19	4,864	0,8031
28	6,127	0,7459

3.1. Solid propellant burning rate at actual rocket motors

Propellant burning rate is mostly influenced by the combustion chamber pressure and is expressed by Saint Robert's (or Vielle's) law within a limited pressure range:

$$r = a \cdot p^n \qquad (1)$$

The pressure exponent *n* and the burn rate coefficient *a* are dependent on chemical composition of a solid propellant and initial temperature of the propellant grain. These coefficients are usually determined by means of a firing test of ballistic evaluation motors [6, 7, 8, 9, 10].

Applied shapes of solid propellant grains for standard ballistic evaluation motors should ensure a low flow velocity over the burning surface or mass flux of combustion products through the internal flow channel. The pressure exponent n should be independent of the combustion chamber pressure at a defined pressure range and should be valid for a defined initial grain temperature.

Burning rate measured by ballistic evaluation motors must be corrected for actual rocket motors, which depends on rocket motor size and conditions of its application. In order to obtain actual values of burning rates within a rocket motor, previous measured values should be fitted for an actual rocket motor. Typical fitting coefficient of burning rates, which is applicable to actual rocket motors, lies between values of 1,01 and 1,05 [7].

Burning rate laws of double base NGR 114 propellant (Figure 14) measured in the standardized 32/16 ballistic evaluation motor at different temperatures are very close to burning rate laws of the NGR 124 double base propellant.

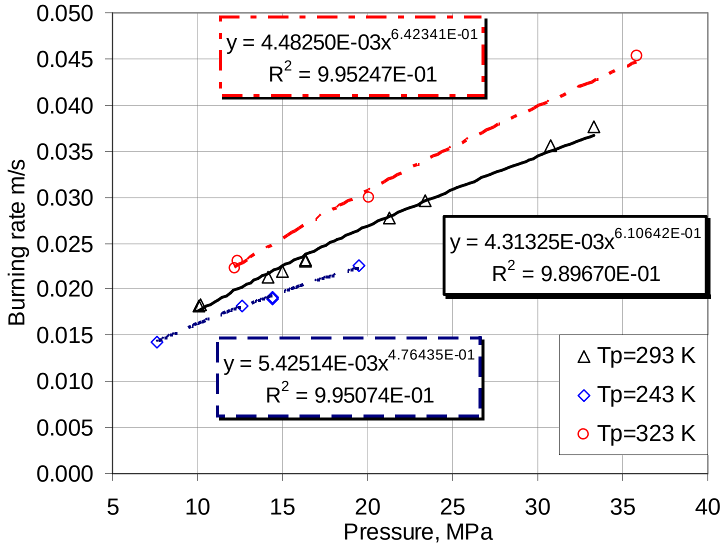

Fig. 14. Burning rate laws of the NGR-114 propellant measured in the standardized ballistic 32/16 type evaluation motor

Actual burning rate within real rocket motors is under other influences and because of that the burning rate is one of ballistic properties, which is determined with difficulty. An actual burning rate in a rocket motor, except the basic value measured in standard ballistic evaluation motors, consists of several components. Determination of these components is a very complex task because many assumptions must be included to estimate their influence on the total actual burning rate.

Estimation of variation of the basic burning rate due to influence of several factors can be made by appropriate separation of each of influencing components. Researches of the influence of gaseous mass flux on the basic burning rate, which were performed by many authors [11, 7], show that combustion products flow over the burning surface causes erosive burning [12, 13].

Influence of mass flux or erosive burning on burning rate in a rocket motor chamber is considered using a modified formula of Lenoir and Robillard (LR). In this model, the total burning rate contains a component of the burning rate in normal burning (no erosive burning) r_0 and a component which is a result of erosive burning r_e [14,20]:

$$r_i = r_0 + r_e \tag{2}$$

The LR model defines the erosive burning contribution as:

$$r_e = \alpha \cdot G^{0,8} \cdot \exp(-\beta \cdot r_b \cdot \rho_s / G) / L^{0,2} \tag{3}$$

$$\alpha = \frac{0.0288 \cdot c_{p_g} \cdot \mu_g{}^{0,2} \cdot \mathrm{Pr}_g^{-2/3}}{\rho_s \cdot c_s} \cdot \left(\frac{T_c - T_s}{T_s - T_0} \right) \tag{4}$$

where G – the mass flux of the combustion gasses, ρ_s – density of propellant [kg/m^3], L – characteristic length [m], c_{pg} – constant pressure specific heat of gasses [J/kgK], Pr – Prandtl number, T_c, T_s, T_0 – temperature of combustion products, burning surface and initial condition of propellant [K], c_s – constant pressure specific heat of propellant [J/kgK]. Using equations 3 and 4, the erosive burning contribution can be calculated using only one empirical value (β), which is essentially independent of propellant composition and approximately 53 [14, 20]. The value of equation 4 can also be assigned from empirical data rather than calculated with transport properties.

Pressure-time predictions for 90 mm M79 and 64 mm M80 rocket motors were performed using the SPPMEF software. Basic burning rate laws of the NGR 114 and NGR 124 double base propellants measured in standardized ballistic evaluation 32/16 type motors (the same burning law for both propellants) were used as an input.

Influence of erosive burning was not included in the first prediction. Considerable deviations of the pressure and burning time were obtained at 243 K (curves $p = f(t)$ with interrupted line) relative to measured values (curves $p=f(t)$ with full line).

When the influence of erosive burning is taken into account (coefficient $J = A_{th}/A_p \approx 0{,}51$) for both rocket motors, following coefficient values were used: β = 65 (for rocket motor 64 mm HEAT M80) and β = 80 (for rocket motor 90 mm HEAT M79), significant curve changes $p = f(t)$ were obtained, comparing to first predictions (Figures 15 and 16). For the 64 mm HEAT M80 rocket motor there are certain differences in the character of prediction and experimental curve $p = f(t)$, and this difference is a result of the ignition process under low temperatures, while for the 90 mm HEAT M79 rocket motor, the curves $p = f(t)$ are very similar.

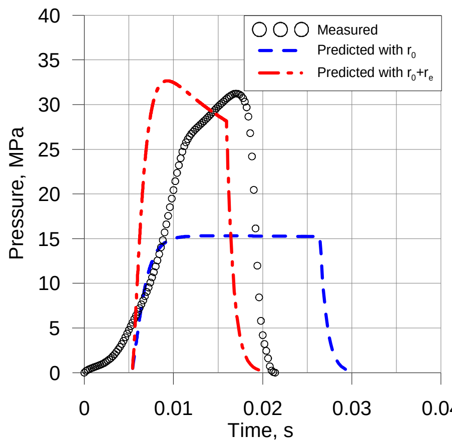

Fig. 15. Pressure vs. time prediction compared with measured curve for a 64 mm HEAT M80 at a temperature of 243 K

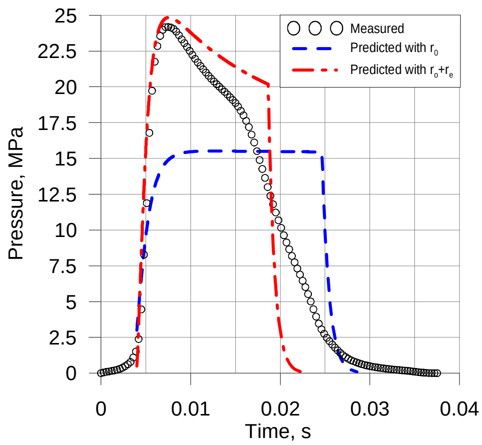

Fig. 16. Pressure vs. time prediction compared with measured curve for a 90 mm HEAT M79 at a temperature of 243 K

Characteristic difference between predicted and measured curves was also confirmed by pressure vs. time prediction at a temperature of 323 K.

The SPPMEF computer software, which was used for these simulations, represents a reliable tool for solid propellant rocket motor performance prediction [15].

Pressure variation in the rocket motor chamber as a function of time is predicted using the following equation:

$$\frac{dp_c}{dt} = \frac{1}{V_{c_i}} \cdot \left[R_g \cdot T_c \cdot \left(\sum_{i=1} \rho_p \cdot A_{b_i} \cdot r_i - \frac{p_{c_i} \cdot A_{th_i}}{C^*} \right) - p_{c_i} \cdot \frac{dV_{c_i}}{dt} \right] \qquad (5)$$

Analysis of equation (5) and curves $p=f(t)$ for rocket motors 64 mm M80 and 90 mm M79 at extreme temperatures shows:

- A crucial influence on pressure variation have the grain burning surface A_{bi} and actual propellant burning rate r_i , while free volume V_{ci} considerable less affects interior ballistic process of the rocket motors.
- Short-action rocket motor structure and solid propellant grain design play important roles during interior ballistic cycle of the rocket motor.
- Deviation of measured curves $p=f(t)$ from predicted curves obtained when the SPPMEF computer software was used, is the result of grain burning surface A_{bi}, and actual propellant burning rate r_i variations (which reflects through erosive burning at some particular zones inside the chamber). This occurs at both rocket motors and during the entire burning process.

Therefore a detailed analysis of all action phases, from the start-up until the tail-off phase was analysed. These deviations can be explained with significant variations of actual solid propellant grain surface A_{bi} when compared with the usual geometric propellant grain burning surface regression model.

A hypothesis that explains mentioned deviations is based on following assumptions:

- During the start-up phase, combustion gases generated by the igniters do not ignite the entire grain surface simultaneously because gaseous flow cannot reach farther zones of inner and outer surfaces of the propellant grain tubes;
- Due to the influence of erosive burning, propellant grain burning surface regression model must be changed to include such a phenomenon;
- The tail-off phase curve deviation occurs because thin partially burned grain tubes are cracked.

In order to confirm this hypothesis a numerical simulation of gaseous flow through the hollow of the propellant grain tubes with gas temperature distribution was carried out. Two cases were considered, one with open tube ends and another with one plugged end. The COMET computer software [16] was used for these simulations.

Results of such simulations (Figure 17.) show that a hot gaseous flow reached the opposite end of the propellant tube in approximately 9 ms at combustion chamber pressure of 9 MPa. Since the total burning time for the analysed rocket motor is about 15 ms, it is obvious that igniters gaseous flow duration in the combustion chamber affects considerably the interior ballistic process in short-action rocket motors. Hot gaseous flow at open propellant grain tube reached the opposite end in about 6 ms.

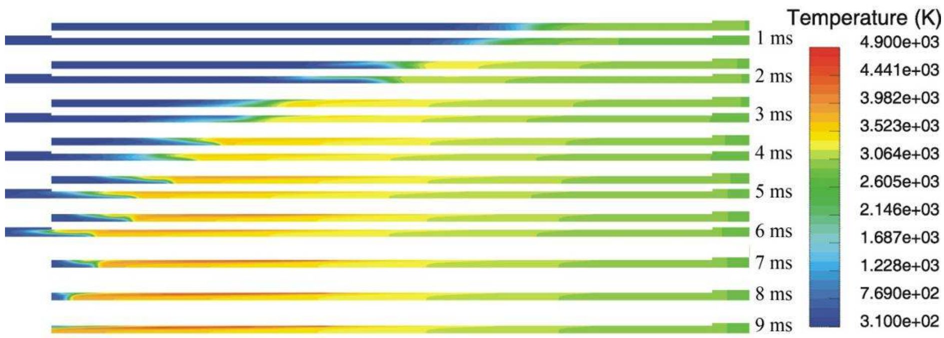

Fig. 17. Hot gaseous flow reach and temperature distribution inside a hollow of tubular propellant grains (for one-end plugged and open propellant tube)

These simulations clearly indicated that a certain delay of ignition at some farther zones of the propellant grain surfaces significantly affects the start-up pressure vs. time curve.

3.2. A model of the corrected propellant grain burning surface

Rocket motors with a high propellant loading factor have also „smothered” burning at outer propellant grain burning surfaces. The presented model of the corrected grain burning surface was based on following "assumptions:

- Start-up phase of short-action rocket motors is a time-consuming process that needs more time for the entire propellant grain surface to be spread with igniter combustion gases. During this transient process only a certain part of the propellant grain surface is burned and other parts of the grain is not yet included into the burning process. It was assumed therefore that total propellant grain surface was ignited when the flame front passed a web burned distance w_i. Length correction of the hollow cylindrical propellant grain (L_0) for inner (L_i^i) and outer (L_i^0) surface was done by means of coefficients k_1 and k_2.
- Total propellant grain surface was spread by the flame when the web burned distance achieved a value of $w_i \geq k_3 \cdot w_0$. This moment was defined by the coefficient k_3.
- Period defined with coefficient $k_4 = 1$, when instantaneous length of the inner and outer burning surfaces of a hollow cylindrical grain became equal.
- A considerable change of burning surface length occurred at a certain moment ($k_4(w_i) < 1$), as shown in Figure 18, because of erosive burning at the start-up phase and non-uniform flame spread along the propellant grain.
- Deviation of the tail-off phase was caused by increased burning surface occurred due to cracks of thin propellant grain remains. Eccentricity of propellant tubes and small web also created conditions for cracks to occur. This also affected the total impulse of the rocket motors.

Burning surface varies in accordance with the following regression model:

$$A_{b_i} = A_{b_i}^o + A_{b_i}^i \tag{6}$$

$$A_{b_i}^o = d_{o_i} \cdot \pi \cdot n \cdot L_i^o \quad and \quad A_{b_i}^i = d_{i_i} \cdot \pi \cdot n \cdot L_i^i \tag{7}$$

$$d_{o_i} = (d_o - 2 \cdot w_i) \quad and \quad d_{i_i} = (d_i + 2 \cdot w_i) \tag{8}$$

$$w_i = \sum r_i \cdot \Delta t_i \tag{9}$$

$$L_i^o = L_0^o \cdot k_1 - w_i \quad and \quad L_i^i = L_0^i \cdot k_2 - w_i \tag{10}$$

where

$$k_1(w_i) \leq 1 \; and \; 0 < k_2(w_i) \leq 1 \; for \; w_i \leq k_3 \cdot w_0, \quad k_3(w_i) \geq 0$$

For $\quad w_i \geq k_3 \cdot w_0 \quad and \quad k_4 = 1$

$$L_i^o = L_i^i = \left(L_0 - w_i\right) \tag{11}$$

For $\quad k_3 \cdot w_0 < w_i \leq w_0 \quad and \quad k_4(w_i) < 1$

$$L_i^o = L_i^i = \frac{w_0 \cdot \left(1 - k_3 \cdot k_4\right) - w_i \cdot \left(1 - k_4\right)}{\left(1 - k_4\right) \cdot w_0} \cdot \left(L_0 - w_i\right) \tag{12}$$

Figure 18 shows a form of the propellant grain burning surface vs. web burned distance according to a presented model.

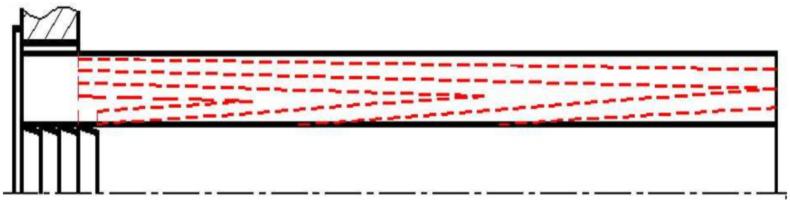

Figure 18. Propellant grain burning surface regression model.

A numerical simulation of curve $p = f(t)$ has been performed for 64 mm M80 „Zolja" and 90 mm M79 „Osa" rocket motors using the above described model of propellant grain burning surface change for short-action rocket motors.

For simulation of the 64 mm M80 „Zolja" rocket motor, coefficients $k_1(w_i)$= 0,3-1,0, $k_2(w_i)$ = 0,3-1,0 (outer propellant grain burning surface was corrected), k_3 = 0,15 and k_4 = 1,0. Within the web range of $k_3 \cdot w_0 < w_i \leq 0{,}5 \cdot w_0$ (for temperature of 243 K ≤ w_0) the coefficient k_4 = 1, and later coefficient $k_4(w_i)$ linearly decreased to the value of k_4 =0,8. For temperature of 243 K coefficient β = 65 and for temperature of 323 K the coefficient β = 58. The obtained functions $p = f(t)$ were very similar to actually measured curves at temperatures of 243 K and 323 K. These agreements are shown in Figure 19 and Figure 20.

There were certain disagreements at the tail-off phase, although further improvement of the corrected propellant grain burning surface model offers an opportunity to achieve better agreements even in this phase.

For simulation of the 90 mm M79 „Osa" rocket motor, coefficients $k_1(w_i)$ = 0,3-1,0, k_2 = 1, k_3 = 0,15 and k_4 = 1,0 (outer propellant grain burning surface was not corrected). Within the web range of $k_3 \cdot w_0 < w_i \leq 0.7 \cdot w_0$ coefficient k_4 = 1 and later coefficient $k_4(w_i)$ linearly decreased to the value of k_4 = 0,75. For temperature of 243 K coefficient β = 80 and for temperature of 313 K coefficient β = 94.

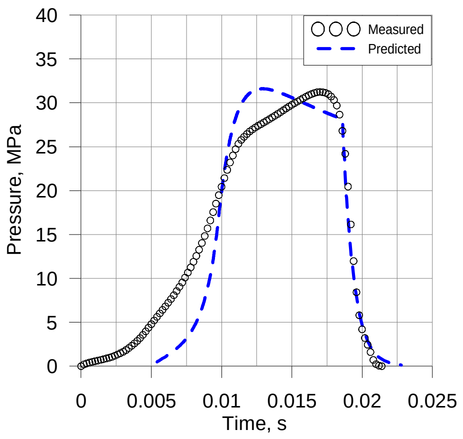

Fig. 19. Comparison of predicted and measured curves at 243 K – 64 mm M80 „Zolja”

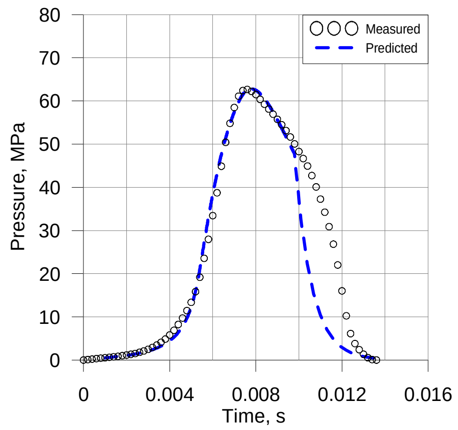

Fig. 20. Comparison of predicted and measured curves at 323 K – 64 mm M80 „Zolja”

Figures 21 and 22 show good agreements of predicted curves with those measured at 243 K and 313 K. As already mentioned, although there were similar disagreements at the tail-off phase, it is possible to achieve better results with further improvement of the corrected propellant grain burning surface model.

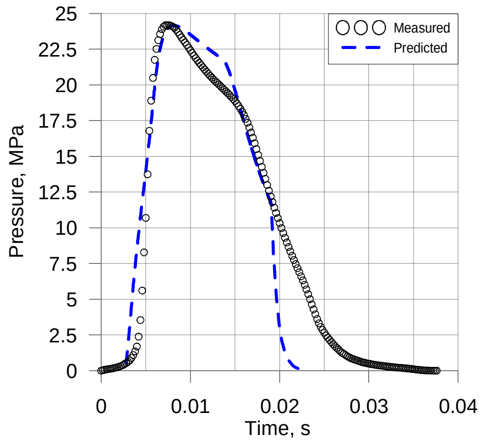

Fig. 21. Comparison of predicted and measured curves at 243 K – 90 mm M79 „Osa”

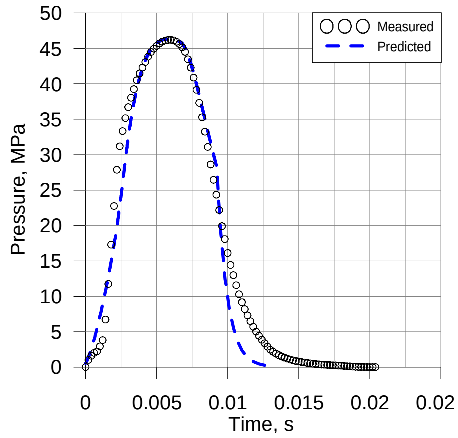

Fig. 22. Comparison of predicted and measured curves at 313 K – 90 mm M79 „Osa”

As illustrated, predictions for a case when length of the outer propellant grain burning surface was not changed were carried out (interrupted line). A considerable deviation of $p=f(t)$ from the measured curve can be noticed (Figure 21).

In this analysis, the total burning surface and cross-sectional throat area ratio represented by K has a value of K = 350 for the 64 mm M80 „Zolja" rocket motor, and K = 326 for the 90 mm M79 „Osa" rocket motor.

The other design ratio J ($J \approx 0{,}52$) for both rocket motors is quite high indicting occurrence of intensive erosive burning.

Gaseous flow velocities at the port zone in the beginning of propellant grain burning were calculated and their values were about 540 m/s for the 90 mm M79 „Osa" rocket motor and about 440 m/s for the 64 mm M80 „Zolja" rocket motor. These values indicate the importance of the role played by the mass flow rate for interior ballistic process of both rocket motors.

For prediction of curve $p = f(t)$ for both impulse rocket motors, it is not possible to use a burning rate determined in standardized 32/16 type ballistic evaluation motors. It is necessary to take into consideration the component of the erosive burning rate (equations 2, 3, 4) and as well as the gas-dynamic effects for specific configuration of propellant charge (non-uniform burning in space and time). We need to introduce numerical simulations of combustion products flowing into free space of the rocket motor. These effects are significant and in certain moments the real burning rate was even twice greater then when it was determined from standardized burning law at higher burning pressures and temperature of 313 K.

4. CONCLUSION

Presented comparative analysis of four short-action solid rocket motors and particularly two (64 mm M80 „Zolja" and 90 mm M79 „Osa") which were mass consumed, shows how their specific features can affect design complexity.

When designed, a short-action solid rocket motor must fulfil the following specific requirements:

- High burning pressure;
- High burn rate;
- „Plateau" burning characteristics in the operating pressure range;
- „Mesa" burning characteristics over the operating pressure range;
- Low temperature sensitivity of the solid propellant (Low π_K);
- Reliable ignition;
- Short time of ignition propellant;
- Short ignition rise time;
- High specific impulse;
- Rocket motor must be operative within the temperature range between −40°C and +60°C.

Design performances of the burst diaphragm affect interior ballistic performances of short-action rocket motors.

A greater thickness of the burst diaphragm can cause combustion oscillations, unforeseen peak pressure and solid propellant grain cracks. Thinner burst diaphragm impedes a proper ignition process which is obvious at the temperature of 233 K (longer ignition rise time) and its influence should be explored as well.

Further research should be focused on more comprehensive igniter gases flow simulation through the inner space of the combustion chamber in order to determine a moment when the entire exposed propellant grain surface was ignited.

Presented method for determination of characteristic points within a burning time, based on derivative dp/dt of measured curve $p = f(t)$ enables that interior ballistic phases and their start and termination moments be more accurately determined.

REFERENCES

[1] http://upload.wikimedia.org/wikipedia/commons/c/c5/AT4_rocket_launcher.jpg

[2] Anon: *APILAS, armour piercing infantry light arm system*, Manurhin et Matra Societe, 1989. http://www.bellum.nu/armoury/GAPILAS.html, http://www.wammt.org/collections/weapons/apilas.htm

[3] http://www.israeli-weapons.com/weapons/missile_systems/anti-armor/b-300/B-300.html

[4] *DRAGON round and tracker, Theory of operation and detailed functional description*, vol. 1, Round, Report no. LO313, Mc Donnell Douglas Astronautics Company, 1978.

[5] Kentgens H., Mackowiak H.P., Schofn R., Short-Action Solid Rocket Motors with Double-Base Propellants, *Propellants, Explosives, Pyrotechnics* 21, 118-126, 1996.

[6] Anon: Solid Rocket Motor Performance Analysis and Prediction, *NASA Report* SP 8039, May 1971, N72-18785.

[7] Fry R.S., *Solid propellant subscale burning rate analysis methods for U.S. and selected NATO facilities*, The Johns Hopkins University, Chemical propulsion information agency, Columbia, Maryland, January 2002

[8] Fry R.S., *Solid propellant test motor scaling*, The Johns Hopkins University, Chemical propulsion information agency, Columbia, Maryland, September 2001.

[9] Terzic J., *Prediction of idealized internal ballistic properties of a rocket motor with DB solid propellant*, Master thesis, University of Sarajevo, Faculty of Mechanical Engineering, 2002.

[10] Zecevic B., *Influence of the variable radial acceleration to internal ballistics of rocket motors with DB propellants*, Dissertation, University of Sarajevo, Faculty of Mechanical Engineering, 1999.

[11] Razdan K.M. and Kuo K.K., Erosive Burning of Solid Propellants, *Fundamentals of Solid-Propellant Combustion*, Edited by Kuo K.K. and Summerfield, Progress in Astronautics and Aeronautics, vol. 90, AIAA, 1984.

[12] Zečević B. and Terzic J., Estimating current burning rate in standard ballistic rocket motor, *Proceedings of 2nd International Symposium, Revitalization and Modernization of Production RIM '99,* Bihać, October 1999.

[13] Zecevic B., Terzic J. and Serdarevic-Kadic S., Effects of kinematics and mass characteristics of gas flow to basic rate burning of double-base rocket propellants, *Proceedings of 3rd International Symposium, Revitalization and Modernization of Production RIM 2001*, Bihać, September 2001.

[14] Willcox M.A., Quinn Brewster M., Tang K.C., Scott Stewart D., and Kuznetsov I., Solid Rocket Motor Internal Ballistics Simulation Using Three-Dimensional Grain Burnback, *Journal of Propulsion and Power* vol. 23, no. 3, May–June 2007.

[15] Terzic J. and Zecevic B., *Prediction of performances of rocket motors. SPPMEF Program*, University of Sarajevo, Defence Technologies Department, 2002.

[16] COMET Version 2.00 — Tutorials, ICCM — Institute of Computational Continuum Mechanics GmbH, Hamburg, March 2001.

[17] http://en.wikipedia.org/wiki/M72_LAW

[18] http://www.armyrecognition.com/forum/viewtopic.php?t=551

[19] http://www.mycity-military.com/Kopnena-vojska/Rucni-Protivoklopni-Raketni-Bacaci-tipa-RPG_4.html

[20] Coats D.E., Levine J.N., Cohen N.S., Nickerson G.R., Tyson T.J., *A Computer Program for the Prediction of Solid Propellant Rocket Motor Performance*, vol. 1, Air Force Rocket Propulsion Laboratory, July 1975.